Journal of Alloys and Compounds 509 (2011) 8073–8076

Contents lists available at ScienceDirect

Journal of Alloys and Compounds

journal homepage: www.elsevier.com/locate/jallcom

Growth and structural properties of pulsed laser-ablated $CuInSe_2$ nanoparticles by pulsed-laser ablation and selenization process

A.R. Jeong[a], W. Jo[a,*], C. Ko[b], M. Han[b], S.J. Kang[c], M. Kim[c], D.Y. Park[d], H. Cheong[d], H.J. Yun[e]

[a] Department of Physics, Ewha Womans University, Seoul 120-750, Republic of Korea
[b] Department of Physics, University of Seoul, Seoul 130-743, Republic of Korea
[c] Department of Materials Science and Engineering, Seoul National University, Seoul 151-742, Republic of Korea
[d] Department of Physics, Sogang University, Seoul 121-742, Republic of Korea
[e] Jeonju Center, Korea Basic Science Institute (KBSI), Jeonju 561-756, Republic of Korea

ARTICLE INFO

Article history:
Received 26 November 2010
Received in revised form 27 February 2011
Accepted 10 May 2011
Available online 24 May 2011

Keywords:
$CuInSe_2$
Nanoparticles
Selenization
Chalcopyrite

ABSTRACT

Nanoparticles of $CuInSe_2$ (CIS) were synthesized by pulsed laser ablation. The effect of the preparation conditions on the structural properties of the CIS nanoparticles was investigated. The CIS nanoparticles showed a more developed structural property after treatment in Se-evaporated atmosphere. By X-ray photoelectron spectroscopy, increase of Se amounts in the CIS nanoparticles was confirmed. Enhancement of phonon modes in the CIS nanoparticles was observed in Raman scattering spectroscopy while secondary phases like In_2Se_3 or CuAu structure-related peak were identified in the spectra. High-resolution transmission electron microscopy indicated that the individual nanoparticles were embedded in matrix of some amorphous layers and diffraction patterns representing the chalcopyrite structure were also scrutinized.

1. Introduction

Chalcopyrite $CuInSe_2$ (CIS)-based materials are most promising for thin-film photovoltaic devices owing to their high absorption coefficient, tunable bandgap that is dependent on the composition and higher efficiency than other thin-film solar cells [1–3].

Although technical studies aimed at improving the performance and decreasing the production cost of CIS solar cell with single-crystal and thin-films CIS have been reported, composition and structure in disperse CIS nanoparticles is not well understood. To improve the solar cell technology in the next generation, it is important to examine the physical mechanisms on the nano-scale. One of the ways is to study physical properties of nanoparticles in terms of phase formation and crystallization.

CIS absorber layers can be prepared using several procedures, such as sputtering [4], electro-plating deposition [5,6], evaporation [7] and the pyrolysis of molecular single-source precursors [8]. Recently, there are some reports about synthesizing CIS nanoparticles by a microwave heating approach [9,10]. Among these, nanoparticle-based chemical reaction deposition has potential due to the advances in nanoparticles synthesis and handling. The major benefit of this method arises from the melting point depression with decreasing nanoparticle size [11]. This study also examined CIS nanoparticles but synthesized by pulsed laser ablation (PLA) and characterized their behavior. PLA has been widely used to make thin-films with multi-elements and demonstrates a powerful tool for growing highly pure and composition-controlled nanoparticles [12–15]. Production rate of nanoparticles by PLA is known as very high [12] and the amounts of nanoparticles are strongly dependent on laser power of the laser. High production yield of nanoparticles can be achieved by a high-power industrial excimer laser. Recently, synthesis of nanoparticles using PLA being done successfully with variety materials by many groups [16,17] while CIS nanoparticles have not been reported yet.

To be used as an absorber in photovoltaic devices, annealing is necessary to improve the electrical properties and to produce polycrystalline CIS materials [5,18]. Several theories have been proposed to explain the re-crystallization step, such as the importance of selenium and copper selenides [5,19,20]. In this study, nanoparticles were synthesized by PLA under different heat treatment conditions, particularly with or without a Se atmosphere.

There are many reports related with structural analysis of Cu–In–Ga–Se thin-films but those of nanoparticles are insufficient. In many cases of CIS-based nanoparticles, they indicate similar results with thin-films [12,21]. However, since it is anticipated that micro-structural change in nanoparticles owing to their decreased size, it is worthy to study detailed analysis of CIS nanoparticles. Furthermore, we can confirm well crystallized nanoparticles from

* Corresponding author. Tel.: +82 2 3277 4066.
E-mail address: wmjo@ewha.ac.kr (W. Jo).

0925-8388/$ – see front matter © 2011 Elsevier B.V. All rights reserved.
doi:10.1016/j.jallcom.2011.05.035

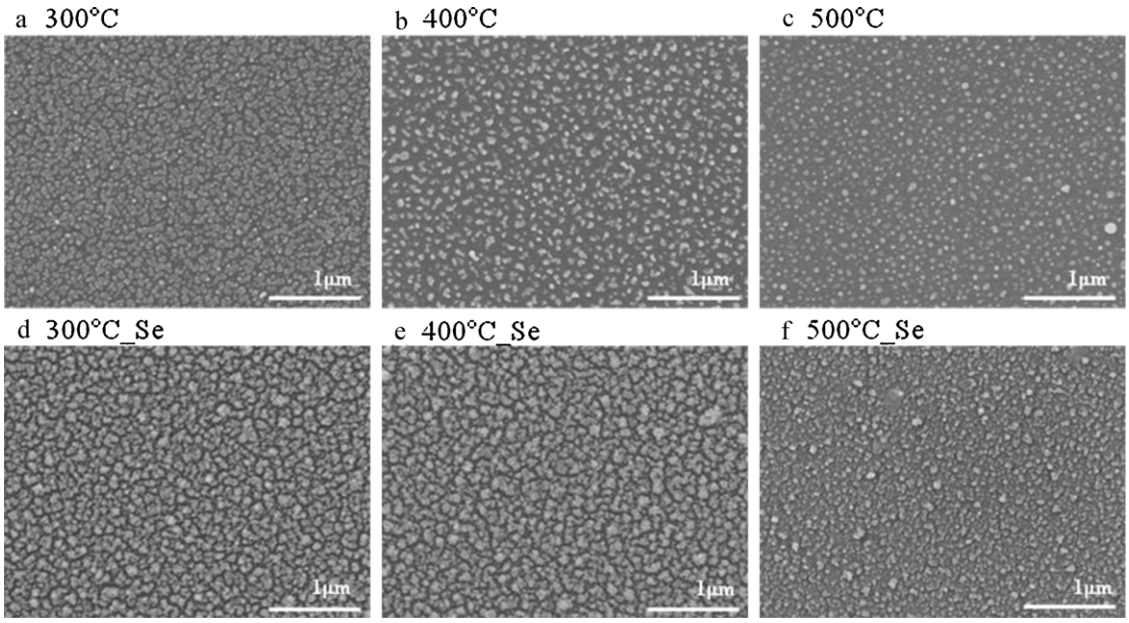

Fig. 1. SEM images of the CIS nanoparticles obtained from pulsed laser ablation and post-thermal treatment (d)–(f) in a vacuum chamber and (a)–(c) under a Se atmosphere at different temperatures.

micro-structural experiment results such as Raman spectra and high-resolution transmission electron microscopy (HR-TEM).

2. Experimental

CIS nanoparticles were synthesized by PLA, which uses a KrF excimer laser with a pulse width and wavelength of 30 ns and 248 nm, respectively. The excitation laser entered the chamber and ablated surface of a rotating stoichiometric CIS target, which has nominal composition of $CuInSe_2$ from a commercial provider.

Ar gas carried the generated nanoparticles to the substrates directly in the PLA chamber. The deposited nanoparticles were thermally treated at various temperatures (300, 400 and 500 °C) for 10 min in vacuum and in selenium atmosphere. Thickness of the nanoparticles layers is 1 μm, which was obtained by 4 h ablation time. From this growth rate, we are able to estimate production yield of the CIS nanoparticle-films as 250 nm/h on a 2 cm × 2 cm of area.

The prepared samples were analyzed by X-ray diffraction (XRD) (Riau, D-Max) with Cu Kα radiation, field emission scanning electron microscopy (FE-SEM) and energy dispersive X-ray spectroscopy (EDS) with an accelerating voltage of 15.0 kV (JSM-6700F, JEOL). X-ray photoelectron spectroscopy (XPS) was performed using an Al Kα (1486.7 eV) source. Before XPS measurement, all samples were Ar^+ ions-sputtered with the beam energy of 2 keV for 2 min in ultra-high vacuum (UHV) to remove surface contamination such as carbon or native oxide. For the samples as-grown and thermally treated in vacuum and in selenium atmosphere, core-level spectra of Cu 2*p*, In 3*d* and Se 3*d* were obtained. The binding energy of photoelectron spectra was calibrated by referring the energy position of C 1s at 248.6 eV. Raman spectroscopy was performed to analyze the detailed structural properties. The size and structural characteristics of the nanoparticle was confirmed by HR-TEM.

3. Results and discussion

Fig. 1 shows SEM images of the CIS nanoparticles obtained after PLA. The particles were treated thermally to improve their crystallinity but they lost Se atoms after the post heat treatment process. To overcome the Se deficiency, they were treated in a Se atmosphere at each temperature, i.e. a selenization process. When the particles were treated in a Se atmosphere, the particles showed greater aggregation than when heat treated in a vacuum. In the case of CIS thin-films, they have been deposited under high temperature over 500 °C to obtain chalcopyrite structure [1,22], the nanoparticles had the chalcopyrite structure despite the low temperature as shown in Fig. 2. The three main peaks in the XRD pattern were assigned to the (1 1 2), (2 2 0)/(2 0 4) and (3 1 2)/(1 1 6) planes of the chalcopyrite structures. Despite the well defined CIS structure, a secondary phase of In_2Se_3 was also observed around $2\theta = 32°$ in XRD.

The results explain the action of Se atoms in crystallization of the CIS nanoparticles which is driven by the defects in this compound. As the formation of interstitial Se is unfavorable in CIS because of high formation energy [23], and selenium anti-sites are also highly energetically unfavorable in ternary. Therefore, incorporation of Se can be accomplished by anion vacancy hopping and exchange mechanisms. The sites would accelerate interdiffusion process in the material and thus enhance crystallization into chalcopyrite structure. Owing to a selenium treatment, acceptor–donor transition can be detected with a sample annealed under high Se pressure since the possible defects induced by a selenium treatment, i.e. $V_{Cu}(A)$, $V_{In}(A)$, $Se_{inter}(A)$, $Se_{In}(A)$, $Se_{Cu}(D)$ and $In_{Cu}(D)$ [5], which means the donor–acceptor transition $Se_{Cu}(D)$–$V_{Cu}(A)$ has been invoked.

Surface chemical analysis of the CIS nanoparticles was examined by XPS. The high-resolution scans of the peaks corresponding to the Cu 2*p*, In 3*d*, and Se 3*d* core levels were performed for the CIS nanoparticles thermally treated in vacuum and in a Se atmosphere.

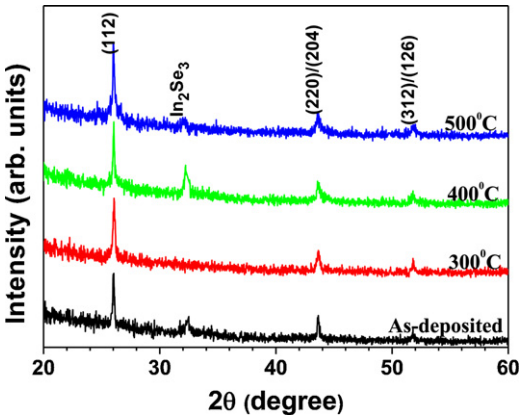

Fig. 2. XRD patterns of the CIS nanoparticles after selenization at different temperatures. The particles were recovered from Se deficiency via the selenization process and indicated a chalcopyrite structure.

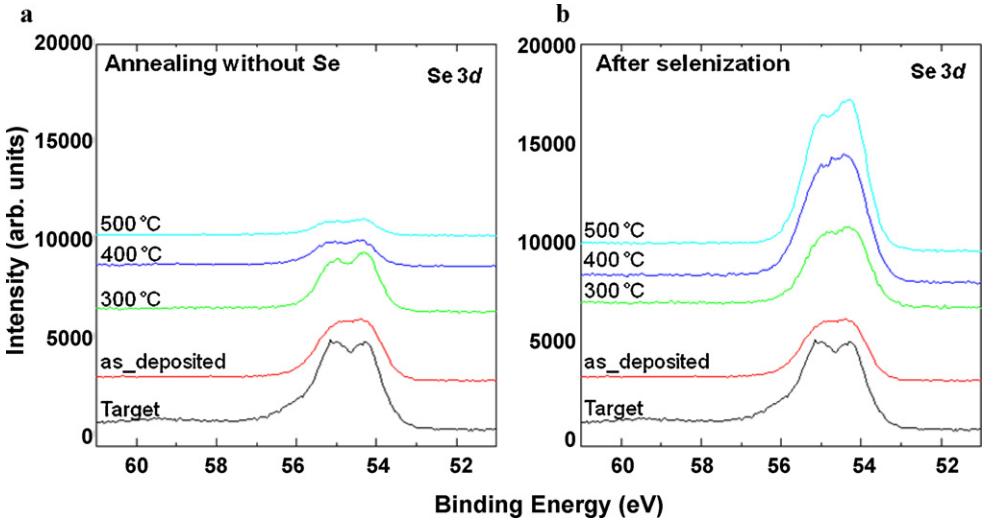

Fig. 3. Se 3*d* core-level spectra of the CIS nanoparticles thermally treated (a) in vacuum and (b) in a Se atmosphere.

Each peak in the binding energies of Cu $2p_{3/2}$, In $3d_{5/2}$ and Se $3d_{5/2}$ was measured at 932.4, 444.6 and 54.3 eV, respectively. The chemical shifts of the binding energies from the reported elements of Cu $2p_{3/2}$, In $3d_{5/2}$ and Se $3d_{5/2}$ were −0.3, +0.6 and −1.3 eV, respectively [24]. It was observed that the thermal treatment little affects the changes of these chemically shifted binding energies. However, we noticed that the peak intensities of binding energies are very sensitive to the thermal treatment conditions. Fig. 3 shows Se 3*d* core level spectra for the as-grown and thermally treated samples in vacuum and in selenium atmosphere. As the treatment temperature rises, the Se 3*d* peak intensity of the samples treated in vacuum is decreased. On the other hand, that of the samples done in selenium atmosphere is increased. This means that the thermal treatment in selenium atmosphere, i.e. the selenization process should be required to overcome the Se deficiency and improve crystallinity of the CIS nanoparticles.

Raman spectroscopy was performed on the CIS nanoparticles produced after selenization at different temperatures. In Fig. 4, all show the A_1 symmetry mode from chalcopyrite ordered at approximately 176 cm^{-1}. This is consistent with previous studies [25–28] where the most intense Raman peak was observed at approximately 175 cm^{-1}. This mode corresponds to anion Se movement with cations at rest.

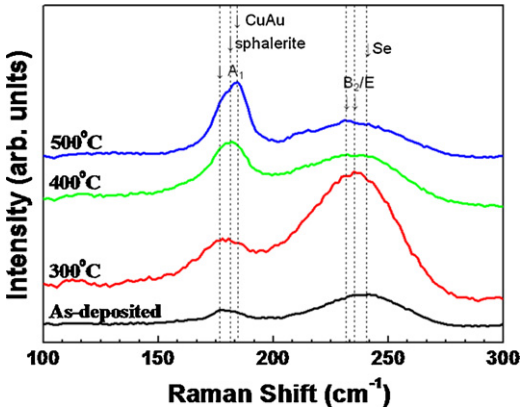

Fig. 4. Raman spectra of the CIS nanopaticles after selenization at different temperatures. The A_1 symmetry mode from chalcopyrite ordered at approximately 176 cm^{-1} coexists with CuAu-ordered CIS at approximately 183 cm^{-1} and the sphalerite structure with an In_2Se_3 second phase at 182 cm^{-1}.

As the annealing temperature is increased, the main peak shifted from 176 to 184 cm^{-1}, which was accompanied by broadening and slight increase in the intensity. This apparent shift of the main peak is due to the appearance of other structures in addition to chalcopyrite. Two crystallographic structures can exist chalcopyrite (α-CIS phase) and disordered sphalerite (β-CIS phase) [26]. Also, quantum mechanical cluster calculations of the crystal structure formation energy in the CIS material system suggest that ordering of the cation sublattices planes along the chalcopyrite [0 1 0] direction in the type-I CuAu structure is almost isenthalpic with the equilibrium chalcopyrite structure [29]. Since the bonding configuration of the nearest neighbors on the lattice is the same in both the chalcopyrite and CuAu structures, the Cu–Se and In–Se bond lengths of both structures are predicted to be almost the same [26]. In-rich CIS has a sphalerite structure with an In_2Se_3 secondary phase, whereas the Cu-rich one has a chalcopyrite structure [28]. Since these nanoparticles are slightly In-rich near surface according to XPS and EDS composition analysis as shown in Table 1(a) and (b), the peak at 182 cm^{-1} may be assigned tentatively to the phonon mode of sphalerite CIS with disordered cations [28]. The discrepancy between XPS and EDS results was caused by penetration depth difference. In other words, atomic sensitivity factor from XPS is the result of detecting near surface about 1–2 nm, but atomic ratio from EDS is that of all stacked nanoparticles. As a result, the A_1 symmetry mode from chalcopyrite at approximately 176 cm^{-1} coexists with CuAu-ordered CIS mode at approximately 185 cm^{-1} [25] and a sphalerite mode with a possible In_2Se_3 secondary phase at 182 cm^{-1} [25,28] forming at stacked nanoparticles surface.

Table 1
Elemental composition of CIS nanoparticles by XPS and EDS.

Annealing temperature (°C)	N_{Cu}/N_{CIS}	N_{In}/N_{CIS}	N_{Se}/N_{CIS}
Target	0.17	0.50	0.33
As deposited	0.18	0.55	0.27
300	0.13	0.62	0.25
400	0.12	0.53	0.35
500	0.10	0.48	0.42

Annealing temperature (°C)	Cu (at%)	In (at%)	Se (at%)
Target	28.92	23.99	47.09
As deposited	40.69	14.47	44.83
300	34.85	19.86	45.29
400	35.22	19.61	45.17
500	36.98	18.13	44.89

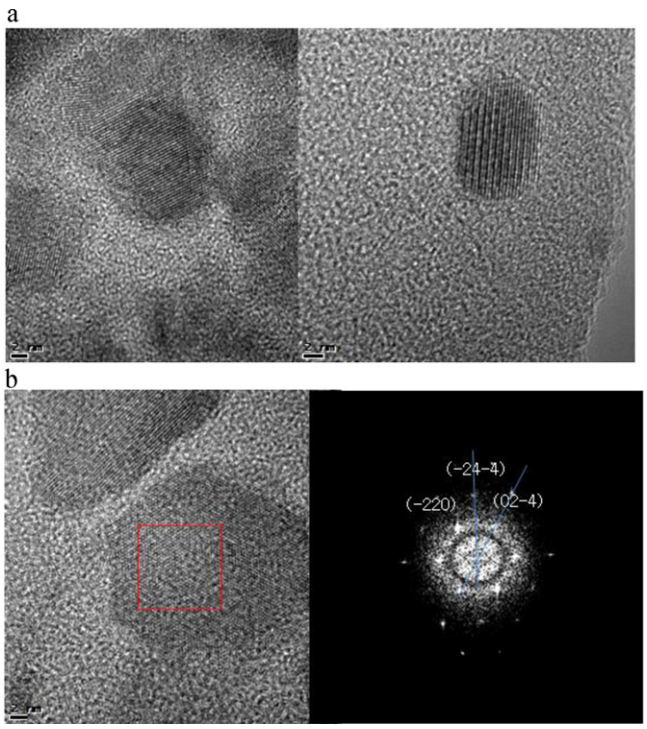

Fig. 5. (a) HR-TEM images of the particles (left) before and (right) after selenization (b) diffraction pattern of CIS nanoparticles after the selenization process.

The Raman spectra are also characterized by a broad feature centered at 240 cm^{-1}. This feature may be ascribed the chalcopyrite B_2 and E modes [28] and/or elemental Se at approximately 240 cm^{-1} [27]. That this feature is strongest for the 300 °C sample suggests existence of surplus Se in the CIS nanoparticles, but this surplus disappeared when the treatment temperature was increased. CIS nanoparticles with an irregular shape easily aggregate together, so the size cannot be defined precisely.

The shape and size of the nanoparticles differed considerably according to heat treatment temperature. The size and microstructure of the product were further examined by HR-TEM, as shown in Fig. 5(a) and (b). The average size of the individual nanoparticle was about 10 nm. They also show different shapes, such as almost spherical and oval shapes, which were attributed to the difference in synthesis conditions. The nanoparticle was formed with one crystal orientation and calculated lattice constant is 5.76 Å which is agreement with 5.754 Å of chalcopyrite CIS. As shown in Fig. 5(b), we confirm that the nanoparticles with chalcopyrite structure were well synthesized under our process according to the FFT pattern.

4. Conclusions

CIS nanoparticles for absorber-layer applications in photovoltaic devices were synthesized by PLA. As-grown CIS nanoparticles were not fully crystallized or stoichiometric. A process of adding Se atoms was required to form more developed structural property and heat treatment in Se-evaporated atmosphere was properly applied. The structure and chemical composition was susceptible to conditions of thermal treatment in the selenization process. By probing the CIS nanoparticles with XRD, Raman spectroscopy, and TEM, it is found that the CIS nanoparticles of chalcopyrite structure are formed through selenization process. It is now important to investigate photovoltaic effects of the CIS nanoparticles with a proper solar cell structure.

Acknowledgments

This study was supported by a grant (code #: 2010K000339) from 'Center for Nanostructured Materials Technology' under '21st Century Frontier R&D Programs' of the Ministry of Education, Science and Technology, Korea.

References

[1] I. Repins, M.A. Contreras, B. Egaas, C. DeHart, J. Scharf, C.L. Perkins, B. To, R. Noufi, Prog. Photovolt Res. Appl. 16 (2003) 235.
[2] N. Rega, S. Siebentritt, J. Albert, S. Nishiwaki, A. Zajogin, MCh. Lux-Steiner, R. Kniese, M.J. Romero, Thin Solid Films 480 (2005) 286.
[3] M.A. Green, K. Emery, Y. Hishikawa, W. Warta, Prog. Photovolt Res. Appl. 17 (2009) 85.
[4] J.A. Thornton, T.C. Lommasson, H. Talieh, B.H. Tseng, Sol. Cells 24 (1998) 1.
[5] J.F. Guillenmoles, A. Lusson, P. Cowache, S. Massaccesi, J. Vedel, D. Lincot, Adv. Mater. 6 (1994) 376.
[6] J.F. Guillenmoles, P. Cowache, A. Lusson, K. Fezzaa, F. Boisivon, J. Vedel, D. Lincot, J. Appl. Phys. 79 (1996) 7293.
[7] A.M. Gabor, J.R. Tuttle, D.S. Albin, M.A. Contreras, R. Noufi, A.M. Hermann, Appl. Phys. Lett. 65 (1994) 198.
[8] S.L. Castro, S.G. Bailey, R.P. Raffaelle, K.K. Banger, A.F. Hepp, Chem. Mater. 15 (2003) 3142.
[9] J.S. Gardner, E. Shurdha, C. Wang, L. Lau, R.G. Rodriguez, J.J. Park, J. Nanopart. Res. 10 (2008) 633.
[10] F. Bensebaa, C. Durand, A. Aouadou, L. Scoles, X. Du, D. Wang, Y. Le Page, J. Nanopart. Res. 12 (2010) 1897.
[11] Y.G. Chun, K.H. Kim, K.H. Yoon, Thin Solid Films 480 (2005) 46.
[12] H.R. Yoon, W. Jo, E.H. Lee, J.H. Lee, M. Kim, K.Y. Lee, Y. Khang, J. Non-Cryst. Solids 351 (2005) 3430.
[13] D.-S. Suh, E. Lee, K.H.P. Kim, J.-S. Noh, W.-C. Shin, Y.-S. Kang, C. Kim, Y. Khang, H.R. Yoon, 1.W. Jo, Appl. Phys. Lett. 90 (2007) 023101.
[14] G.-S. Park, J.-H. Kwon, M. Kim, H.R. Yoon, W. Jo, T.K. Kim, J.-M. Zuo, Y. Khang, J. Appl. Phys. 102 (2007) 013524.
[15] A.R. Jeong, H.R. Yoon, Y.J. Oh, T.Y. Kim, W. Jo, M. Kim, J. Nanosci. Nanotechnol. 9 (2009) 901.
[16] H. Zeng, W. Cai, J. Hu, G. Duan, P. Liu, Y. Li, Appl. Phys. Lett. 88 (2006) 171910.
[17] B. Liu, Z. Hu, Y. Chen, X. Pan, Appl. Phys. Lett. 90 (2007) 044103.
[18] D. Lincot, J.F. Guillemoles, S. Taunier, D. Guimard, J. Sicx-Kurdi, A. Chaumont, O. Roussel, O. Ramdani, C. Hubert, J.P. Fauvarque, N. Bodereau, L. Parissi, P. Panheleux, P. Fanouillere, N. Naghavi, P.P. Grand, M. Benfarah, P. Mogensen, O. Kerrec, Sol. Energy 77 (2004) 725.
[19] R. Klenk, T. Walter, H.W. Schock, D. Cahen, Adv. Mater. 5 (1993) 114.
[20] M.S. Sadigov, M.O¨. Zkan, E. Bacaksiz, M. Altunbas, A.I. Kopya, J. Mater. Sci. 34 (1999) 4579.
[21] J. Olejnïček, C.A. Kamler, A. Mirasano, A.L. Martinez-Skinner, M.A. Ingersoll, C.L. Exstroma, S.A. Darveau, J.L. Huguenin-Love, M. Diaz, N.J. Ianno, R.J. Soukup, Sol. Energy Mater. Sol. Cells 94 (2010) 8.
[22] C. Calderón, P. Bartolo-Pérez, G. Gordillo, Phys. Status Solidi C 1 (2004), No. S1.
[23] G. Dagan, F. Abou-Elfotouh, D.J. Dunlavy, R.J. Matson, D. Cahen, Chem. Mater. 2 (1990) 286.
[24] J.F. Moulder, W.F. Stickle, P.E. Sobol, K.D. Bomben, Handbook of X-ray Photoelectron Spectroscopy, Reissue edition, Physical Electronics Inc., 1995 (February).
[25] X. Fontane, V. Izquierdo-Roca, L. Calvo-Barrio, J. Alvarez-Garcia, A. Perez-Rodriguez, J.R. Morante, W. Witte, Appl. Phys. Lett. 95 (2009) 121907.
[26] B.J. Stanbery, S. Kincal, S. Kim, C.H. Chang, S.P. Ahrenkiel, G. Lippold, H. Neumann, T.J. Anderson, O.D. Crisalle, J. Appl. Phys. 91 (2002) 3598.
[27] V. Izquierdo-Roca, E. Saucedo, C.M. Ruiz, X. Fontane, L. Calvo-Barrio, J. Alvarez-Garcia, P.P. Grand, J.S. Jaime-Ferrer, A. Perez-Rodriguez, J.R. Morante, V. Bermudez, Phys. Status Solidi A 206 (2009) 1001.
[28] S. Shirakata, H. Kubo, C. Hamaguchi, S. Isomura, Jpn. J. Appl. Phys. 36 (1997) L1394.
[29] S.H. Wei, L.G. Ferreira, A. Zunger, Phys. Rev. B 45 (1992) 2533.